Journal of Materials Chemistry A

ROYAL SOCIETY OF CHEMISTRY

REVIEW

View Article Online
View Journal | View Issue

Cite this: J. Mater. Chem. A, 2023, 11, 20368

Reticular chemistry within three-dimensional covalent organic frameworks for multiple applications

Xiaokang Wang, Fei Gao, Zixi Kang, Weidong Fan * and Daofeng Sun *

Compared with two-dimensional (2D) covalent organic frameworks (COFs), three-dimensional (3D) COFs have significant advantages, such as larger specific surface areas, complex interconnected structures, and fully accessible active sites, which have aroused extensive interest of researchers. With the rapid development of various 3D COFs, they exhibit great application prospects in many fields, including but not limited to gas storage and separation, catalysis, fluorescence, batteries, conductivity, and drug delivery. Herein, we summarize the advances in the rational design and synthesis of 3D COFs guided by reticular chemistry and topology to explore potential unexploited structures and provide an overview of recent progress in their multifunctional applications, aiming to expand the potential of 3D COFs in practical applications.

Received 25th July 2023
Accepted 11th September 2023

DOI: 10.1039/d3ta04395a

rsc.li/materials-a

Introduction

As an emerging class of crystalline porous materials, covalent organic frameworks (COFs) are composed of multifunctional organic building units connected *via* strong covalent bonds to generate two-dimensional (2D) layered structures or three-dimensional (3D) interconnected networks.[1–3] Due to the advantages of low density, high porosity, and designable functionality, COFs have attracted great interest and shown versatile application potential in gas storage and separation,[4–6] catalysis,[7–9] sensing,[10–12] energy storage,[13–17] and so on.[18–21] Compared with one-dimensional (1D) channels in 2D COFs, more complex pore structures, such as interpenetrated channels and cages, were observed in 3D COFs.[22–26] Moreover, higher surface area, lower density, and abundant accessible active sites also make 3D COFs more suitable than 2D COFs for practical applications.

However, most current research efforts are still focused on the fields of 2D COFs,[27–29] and the progress of 3D COFs is still in the infancy due to the limited availability of 3D organic building units and difficulty in structural determination, especially for those with new topologies or dynamics. For example, most reported 3D COFs are constructed with monomers of tetrahedral (T_d) symmetry,[30–32] with only a few exceptions of triangular (C_3),[33] square (C_4),[34] triangular prism (D_{3h}),[35] and cubic (O_h) symmetry.[36] In addition, serious crystallization problems and relatively lower stability due to large voids and a lack of strong π–π stacking are also bottlenecks for 3D COFs.[37] Without the limitation of layered structures, the more flexible orientation of building units may lead to the preference of amorphous products rather than crystalline structures.

Despite these issues, considerable efforts have been devoted to the design, preparation and application of 3D COFs (Fig. 1), and great progress has been made since they were first reported by Yaghi and co-workers in 2007 due to the tremendous development of reticular chemistry,[30] which greatly improved the ability of structural and functional design. Over the past few decades, there have been many reviews on 2D COFs, but relatively few on 3D COFs. Wang *et al.* reviewed the key strategies

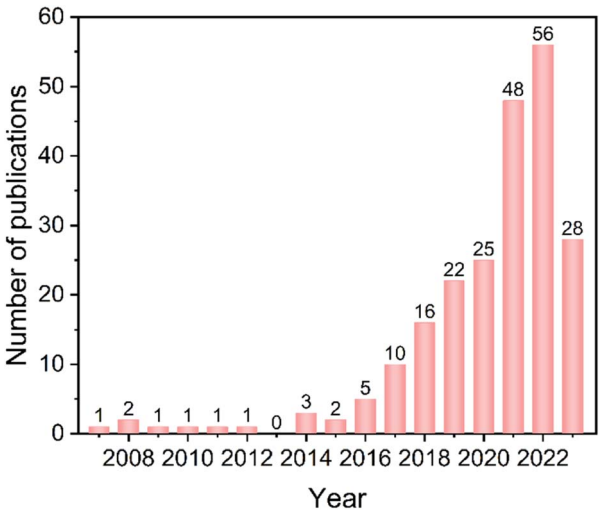

Fig. 1 Growth trend in research on 3D COFs from 2007 to 2023. Data obtained from the Web of Science on July 10th, 2023.

State Key Laboratory of Heavy Oil Processing, School of Materials Science and Engineering, China University of Petroleum (East China), Qingdao, Shandong 266580, China. E-mail: wdfan@upc.edu.cn; dfsun@upc.edu.cn

and technologies for the structure design and determination of 3D COFs.[38] Fang *et al.* summarized the design principles, functional approaches, and stability regulation methods of functional 3D COFs.[39–41] Nguyen *et al.* discussed the growth mechanism and different topological structures of 3D COFs with T_d building blocks.[42] These reviews have aroused great interest in the design, synthesis, structure, and applications of 3D COFs. Herein, we summarize the advances in the rational design and synthesis of 3D COFs under the guidance of reticular chemistry and topology and give a brief overview of recent progress in their versatile applications in gas storage and separation, catalysis, fluorescence, batteries, conductivity, and drug delivery. Finally, we discuss the challenges and perspectives of 3D COFs for future applications.

Reticular chemistry and topology

Reticular chemistry, with its concepts of modularity and predictability, offers a powerful approach for the design and synthesis of crystalline porous materials.[43–45] With the combination of dynamic covalent chemistry, COFs with periodic networks of organic monomers linked by covalent bonds are obtained.[46] The structure and properties of COFs are directly related to the symmetry and connectivity of the monomers used. Therefore, the rational design of monomers is crucial for the design of COFs. Generally, monomers with high connectivity are conducive to the formation of 3D COFs. So far, 4-connected building blocks based on tetraphenylmethane and adamantane derivatives,[30] 6-connected building blocks based on triptycene,[47] organic cages,[35] and polycyclic aromatic hydrocarbons,[48] and 8-connected building blocks based on borophosphonates,[36] pentiptycene,[49] porphyrin,[50] *etc.* have been applied in the design and construction of 3D COFs.

Topology is one of the critical issues in 3D COFs, which may affect the selection of suitable building blocks, intrinsic aperture characteristics, and potential applications.[51] Under the guidance of reticular chemistry, thousands of possible topological structures in 3D COFs can be theoretically predicted according to the Reticular Chemistry Structure Resource (RCSR) database.[52] However, only 29 topologies (*ctn*,[30] *bor*,[30] *dia*,[53] *pts*,[54] *rra*,[55] *ffc*,[33] *lon*,[31] *srs*,[56] *acs*,[35] *bcu*,[36] *fjh*,[57] *stp*,[47] *tbo*,[34] *ceq*,[58] *hea*,[59] *ljh*,[32] *nbo*,[60] *pcu*,[48] *soc*,[61] *flu*,[62] *pcb*,[50] *scu*,[63] *she*,[64] *spn*,[65] *sql-c*,[66] *lvt*,[67] *mhq-z*,[68] *pto*,[68] and *tty*[69]) have been reported in 3D COFs to date (Fig. 2), with numerous 3-periodic topologies to be further

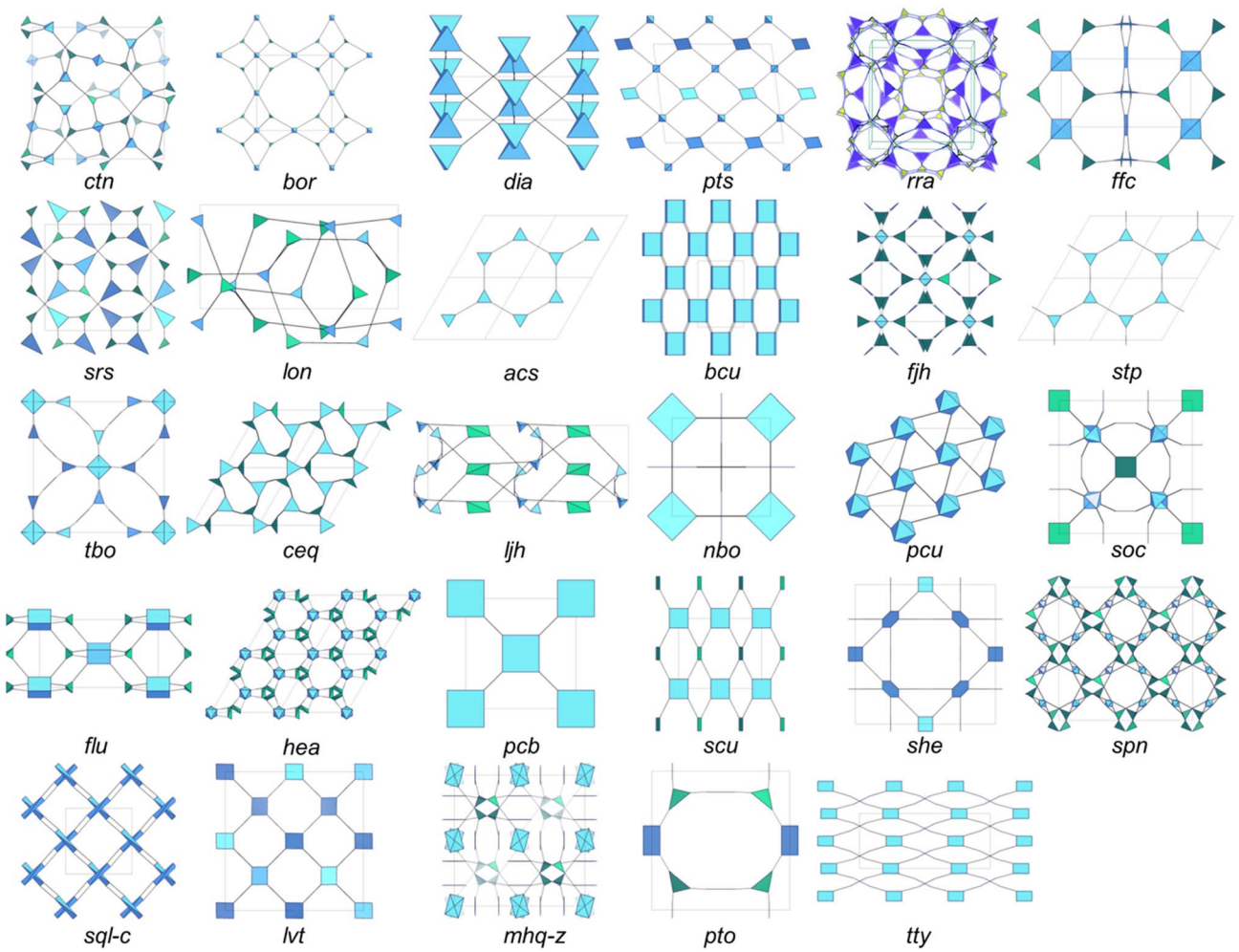

Fig. 2 Reported topologies in 3D COFs.

Table 1 Summary of discovered topologies in 3D COFs

3D COFs	Topology	Connectivity	Symmetry	Time	Pore size (Å)	Pore volume ($cm^3\ g^{-1}$)	BET surface area ($m^2\ g^{-1}$)	Applications	Ref.
COF-102	*ctn*	[4 + 3]	$T_d + C_3$	2007	8.9	1.35	3472	—	30
COF-108	*bor*	[4 + 3]	$T_d + C_3$	2007	15.2, 29.6	—	—	—	30
COF-300	*dia*	[4 + 2]	T_d + linear	2009	7.8	0.72	1360	—	53
3D-Py-COF	*pts*	[4 + 4]	$T_d + C_2$	2016	5.9	0.72	1290	Fluorescence	54
CD-COFs	*rra*	[8 + 4]	$T_d + C_8$	2017	6.4	0.39	760	Conductivity	55
3D-ETTA-TFPA	*ffc*	[4 + 3]	$C_3 + C_2$	2018	17.3	0.75	1174	—	33
LZU-111	*lon*	[4 + 4]	$T_d + T_d$	2018	10.9	0.918	2120	—	31
SiCOF-5	*srs*	[3 + 3]	$C_3 + C_3$	2018	—	—	370	—	56
3D-CageCOF-1	*acs*	[6 + 2]	D_{3h} + linear	2020	5.1, 8.5	0.5	1040	Gas adsorption	35
BP-COF-1	*bcu*	[8 + 2]	O_h	2020	6	—	519	—	36
COF-790	*fjh*	[4 + 3]	$C_2 + C_3$	2020	21.5	—	2650	—	57
JUC-564	*stp*	[6 + 4]	$D_{3h} + C_2$	2020	43	—	3383	—	47
COF-1	*tbo*	[4 + 3]	$C_4 + C_3$	2020	14, 20, 33	—	—	Photocatalysis	34
3D-*ceq*-COF	*ceq*	[6 + 3]	$D_{3h} + C_3$	2021	10, 16	—	1148.6	Gas adsorption	58
3D-*hea*-COF	*hea*	[6 + 4]	$D_{3h} + T_d$	2021	16	—	1804	Gas separation	59
3D-TPB-COF-Ph	*ljh*	[4 + 4]	$T_d + C_2$	2021	10	—	1430	—	32
SPB-COF-DBA	*nbo*	[4 + 4]	D_{4h}	2021	24.5	0.9	1726	—	60
Marta-COF-3	*pcu*	[6 + 2]	D_{3d} + linear	2021	6	—	778	Charge transport	48
Ti-COF-1	*soc*	[6 + 4]	$C_3 + C_2$	2021	16	—	1000.4	Photocatalysis	61
NKCOF-36	*flu*	[8 + 4]	$D_{2h} + T_d$	2022	6, 9	0.23	1093	Gas separation	62
NUST-5	*pcb*	[8 + 2]	D_{4h} + linear	2022	10, 15	—	680	Photocatalysis	50
TUS-84	*scu*	[8 + 4]	$D_{2h} + C_4$	2022	9.7	0.7613	679	Drug delivery	63
TAPP-HFPB-COF	*she*	[6 + 4]	$D_{4h} + C_6$	2022	20	—	1060	Photocatalysis	64
TiCOF-*spn*	*spn*	[6 + 3]	$C_3 + C_3$	2022	14.1, 27	—	621.38	Photocatalysis	65
COF-39	*sql-c*	[4 + 2]	C_2 + linear	2022	25	—	813	—	66
DDHP-COF	*lvt*	[4 + 4]	$C_2 + C_2$	2023	19.4	0.88	1679	Conductivity	67
RICE-7	*mhq-z*	[4 + 3]	$C_3 + C_2$	2023	10	—	1448	Gas adsorption	68
RICE-3	*pto*	[4 + 3]	$C_3 + C_2$	2023	10, 14, 32, 46	—	720	Gas adsorption	68
COF-NUST-16	*tty*	[8 + 4]	$D_{2h} + C_2$	2023	16	—	876.7	Photocatalysis	69

explored. The discovery timing and characteristics of corresponding 3D COFs are summarized in Table 1.

Since first reported in 2007, *ctn* and *bor* topologies have been realized in 3D COFs using building blocks with T_d and C_3 symmetries.[30] Replacing the triangular building blocks with linear precursors provides the *dia* topology, which is the most common topology in 3D COFs.[53] Only these three topologies were achieved in the first decade by Yaghi *et al.*[30,53] due to the limitation of the topology design strategy and the lack of building blocks with high connectivity. In 2016, Wang *et al.* proposed a new strategy to design COFs *via* a [4 + 4] reaction of tetrahedral and quadrilateral precursors and successfully obtained 3D-Py-COFs with the fourth *pts* topology.[54] However, the above topologies contain at least one T_d monomer, which is adverse to the structural diversity of 3D COFs. Zhong *et al.* constructed the first 3D COFs using 2D building blocks with triangular and square symmetry in 2018.[33] Cooper *et al.* synthesized a 6-connected organic cage molecule with D_{3h} symmetry as a building block to provide the first cage-based 3D COF in 2020.[35] In the same year, Yaghi *et al.* demonstrated the feasibility of constructing 3D COFs with 8-connected nodes.[36] Thereafter, several new topologies have been realized by controlling the connectivity of building blocks under the guidance of reticular chemistry. Therefore, reticular chemistry has become a frequently discussed topic and an inevitably unique concept in COF structural design and engineering. In particular, the rational design of new structures, the exploration of novel topologies, reticular expansion, and post-synthetic modification (PSM) are all included in this concept, which is crucial for the diversity of the COF structural library and further influences the chemistry and applications of 3D COFs. In other words, the rich chemical properties of 3D COFs largely depend on the comprehension of reticular design, which conversely realizes the optimal correlation between the structure of 3D COFs and their performance in practical applications.

There is no doubt that a comprehensive understanding of topology is crucial for the design and synthesis of novel 3D COFs with diverse structural types. There are two different strategies to obtain targeted 3D COFs, one of which is the assembly of supermolecules by controlling the arrangement of building blocks. The flexible conformation of organic bonds determines the multiple orientations of the building blocks and makes them difficult to adjust for predictable specific topologies. Another one is the employment of rigid polyhedral building blocks, such as tetrahedra, trigonal prisms, and octahedra. These predesigned building blocks allow further combinations guided by reticular chemistry to form prefabricated topologies. In other words, it is feasible to precisely control the structural types of 3D COFs by considering the preferred topology based on the connectivity and shape of specific building blocks.

The structural design and discovery of 3D COFs with different topologies are mainly based on the geometry and conformation of the building blocks. The geometry of building blocks plays an

essential role in the construction of target frameworks based on reticular chemistry, such as *ctn*, *bor*, *pts*, *etc*, whereas the geometric conformation of building blocks is the most effective method for selectively crystallizing specific topological structures, such as *fjh* and *ljh*. Consequently, based on the concept of reticular chemistry, a comprehensive exploration of reticular design is of practical significance for the structural design of 3D COFs. Generally, the reticular synthesis of 3D COFs contains five steps: (i) selection of the desired topology and partitioning the framework by slicing edges into vertices; (ii) analysis of geometry, precise angles, and vertices based on the number of points required for expansion; (iii) recognition of molecular equivalent vertices with large rigid polyaromatic molecules as building blocks for predicting precise geometric structures; (iv) connection of building blocks *via* covalent bonds to generate COFs by tuning the reaction kinetics and reversibility between building blocks at the microscopic scale; (v) confirmation of the network structure with a clear understanding of the precise architecture of vertices.

To sum up, reticular chemistry utilizing the geometry and conformation of building blocks has been demonstrated to be an effective and important strategy, which enables predictions of the way small organic molecules may assemble into macroscopic 3D COFs with periodic structures and diverse topologies. Therefore, reticular chemistry provides a target-oriented approach for synthesizing 3D COFs with atomically precise predesigned architectures. Essentially, the main advantage of reticular chemistry in 3D COFs is the ability to fabricate new frameworks by tuning the size and functionality of the building blocks, resulting in the same topology but with different pore sizes and functions (Fig. 3). Various building blocks offer numberless design possibilities, and distinct combinations and connectivity patterns enable the discovery of new topologies within 3D COFs. Meanwhile, the usage of building blocks with short size can produce structures with smaller pores for a given topology, while larger pores can be obtained with longer building blocks. The facile embedding of multiple functional groups in the building blocks endows the framework with highly functional characteristics. The enormous design potential and rich functionalities of reticular chemistry boost the versatility of 3D COFs, *i.e.* almost infinite reticular 3D COFs can be predesigned and subsequently edited internally and externally.

Synthetic methods

As discussed above, limited building units have been used to construct 3D COFs, and the synthesis of 3D COFs with high crystallinity remains challenging.[70–72] Appropriate synthesis conditions, such as temperature, pressure, time, and solvent composition, are crucial for the crystallization of 3D COFs. In this section, several synthetic methods for 3D COFs are summarized, including solvothermal synthesis, microwave-assisted synthesis, plasma-induced synthesis, ionothermal synthesis, deep eutectic solvent-assisted synthesis, self-addition synthesis, modulator-assisted synthesis, cosolvent-assisted synthesis, and supercritical solvothermal synthesis.

Synthesis of powder 3D COFs

Currently, the obtained 3D COFs are almost in the form of powders with the widely used solvothermal synthesis method. Considering the drawbacks faced in solvothermal synthesis, such as long reaction time, high temperature, and complex operation, other synthetic methods using different energy sources and reaction media are being developed, but are still at the starting stage with rather few instances.

Since first reported by Yaghi *et al.* in 2007,[30] solvothermal synthesis has become the most common method for the preparation of 3D COFs. In this way, precursors are added to solvents with appropriate compositions and sealed in a Pyrex tube to be heated at high temperatures (120 to 160 °C) for a long time (3 to 7 days). After cooling to ambient temperature, 3D COFs are obtained through filtration and further purified by washing with suitable solvents or Soxhlet extraction. In solvothermal synthesis, temperature, time, and solvent

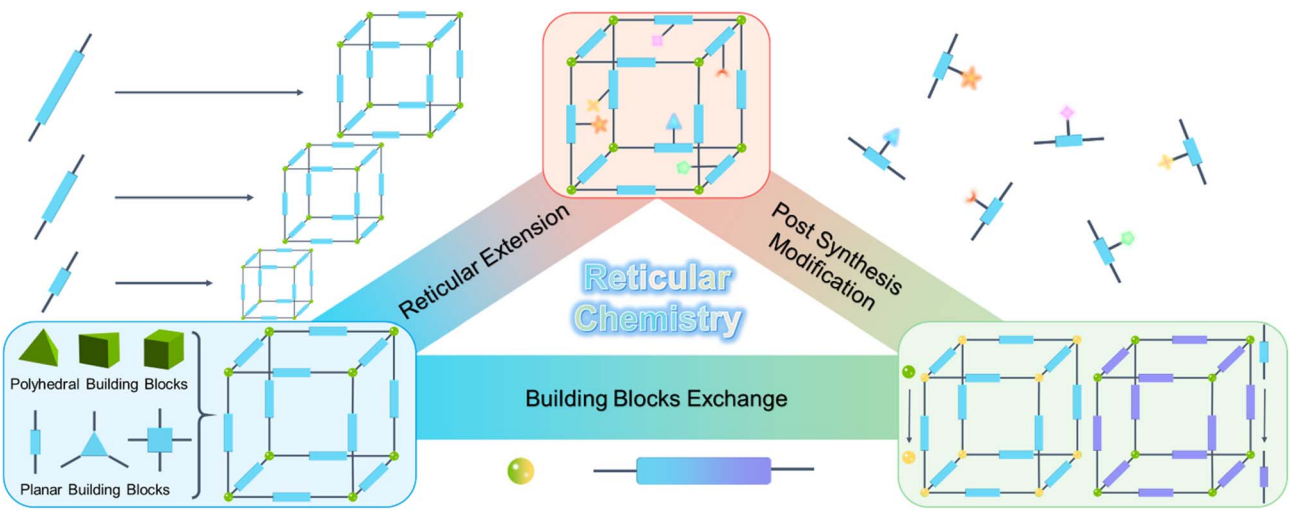

Fig. 3 Schematic illustration of reticular chemistry in 3D COFs.

composition of the reaction systems have a significant effect on the crystallinity and porosity of 3D COFs.

Microwave-assisted synthesis has been widely used in synthesis as a modified solvothermal synthesis method with microwave heating. Compared with traditional solvothermal synthesis, microwave heating has the advantages of accelerated reaction speeds, high yields, clean products, and low energy consumption. For example, Cooper *et al.* reported the synthesis of COF-102 with microwave irradiation at 100 °C and a power of 200 W in 20 min.[73] N_2 adsorption isotherm, powder X-ray diffraction (PXRD), and Fourier transform infrared (FTIR) data of obtained COF-102 were comparable to those published previously.

Other extra energy sources, *e.g.* plasma, can also be utilized for the synthesis of 3D COFs. As a typical atmospheric pressure non-equilibrium plasma, liquid dielectric barrier discharge (DBD) plasma with the benefits of a simple structure, low consumption, and ambient operation can promote many reactions that are difficult to occur. In 2021, Hou *et al.* demonstrated the use of liquid DBD plasma for a green, rapid, facile and energy-saving synthesis of COF-102 in 10 min under atmospheric pressure without inert gas protection.[74] The reaction rate was over 400 times faster than the reported time of 72 h for solvothermal synthesis.

As organic salts with low melting points, ionic liquids (ILs) are composed solely of liquid phase ions and have attracted extensive attention in recent years as a green and safe reaction medium due to their unique characteristics, such as good solubility, incombustibility, negligible vapor pressure, a wide liquid range, and a highly designable structure. In 2018, Fang *et al.* proposed the fast ionothermal synthesis of 3D-IL-COFs under ambient conditions with 1-butyl-3-methylimidazolium bis((trifluoromethyl)sulfonyl)imide ([BMIm][NTf_2]) as solvent and a catalyst.[75] These 3D-IL-COFs can be produced within 12 h, while the synthesis of highly crystalline 3D-IL-COF-1 can be realized within 3 min. In addition, [BMIm][NTf_2] can be reused at least three times without losing activity after simple filtration, presenting a potential pathway for the green and large-scale synthesis of 3D COFs.

Another green medium is deep eutectic solvent (DES) formed through strong hydrogen bond interactions between a hydrogen bond donor (HBD) and hydrogen bond acceptor (HBA). DESs can be prepared *via* a simple stir of corresponding HBDs and HBAs at room temperature without by-products. Compared with ILs, DESs also have the significant advantages of non-toxicity, low price, and good biodegradability. In 2020, Wang *et al.* reported the synthesis of 3D-COF-1 and 3D-COF-HNU10 with choline chloride (ChCl) and glycerol (Gly) as solvents under ambient conditions.[76] 3D-COF-1 with high crystallinity was available within only 2 h in ChCl/Gly (1 : 2), and 3D-COF-HNU10 with azo groups was obtained in 24 h, which was unavailable for the solvothermal synthesis method.

Synthesis of single-crystal 3D COFs

It is difficult to determine the structure of 3D COF powders, especially when they are not based on the expected framework. In addition, the coarse crystal structure obtained through PXRD combined with structural simulation usually lacks atomic positions and geometric parameters. The growth of single crystals may provide a perfect solution to these problems, but it is difficult to realize, which makes the development of a universal and facile method for 3D COF single crystals a research hotspot.

The first case of 3D COFs that can be fully characterized by single-crystal X-ray diffraction (SCXRD) was reported by Wuest *et al.* in 2013.[77] Large and uniform micron-sized monocrystalline NPN-1, NPN-2, and NPN-3 with *trans* azodioxide linkages were obtained *via* the self-addition polymerization of tetranitroso monomers at room temperature, and the size of NPN-3 even approached 0.5 mm (Fig. 4a). This work was a successful example, but it was only limited to rare azodioxide linkages. Yaghi *et al.* also reported the solvothermal synthesis of single-crystal COF-320 of $1.0 \times 0.5 \times 0.2$ μm^3 in the same year.[78] However, the too small size only allowed for structure resolution *via* single-crystal 3D electron diffraction using the rotation electron diffraction (RED) method, which provided a powerful tool for the structural determination of microcrystalline COFs.

In 2018, Wang *et al.* proposed the modulator-assisted synthesis of large single crystal imine-based COFs, including COF-300, COF-303, LZU-79, and LZU-111.[31] They chose aniline as a modulator to increase the formation reversibility of imine bonds and enhance the process of error correction through the imine exchange strategy (Fig. 4b). The size of single-crystal COFs was controllable through the adjustment of aniline dosage, *e.g.* 10–60 μm for COF-300 with 0.005–0.12 mL aniline. However, this method was constricted by the long reaction time, such as 30–40 days for COF-300 of 60 μm.

Dichtel *et al.* synthesized 3D boroxine-linked single-crystal TMPh-COF based on tetraphenylmethylboronic acid with nitriles as cosolvent in 2019.[79] Electron-donating nitriles could stabilize the boroxine-linked COFs into a colloidal suspension due to the interaction between nitriles and boron-containing functional groups in the framework, which was also inapplicable to other systems.

As a special medium, supercritical fluid exhibits greatly enhanced mass transfer due to its unique characteristics, such as gas-like diffusion rate, liquid-like density, viscosity, surface tension, and solvation, and can realize green, scalable and efficient preparation that cannot be achieved in normal media. Wei *et al.* reported the first case of 3D single-crystal COFs within minutes with supercritical carbon dioxide (sc-CO_2) as a solvent in 2022 (Fig. 4c).[80] The crystal growth rate of 3D COFs reached 35 μm min^{-1}, and a single crystal of up to 110 μm was formed in 1–5 min, which was 2–5 orders of magnitude faster than that of solvothermal or ionothermal synthesis (Fig. 4d).

In summary, solvothermal synthesis is still the mainstream synthesis method for 3D COFs, which is generally applicable to almost all reported linkages but suffers from the disadvantages of long reaction time, high temperature, and large solvent consumption for excellent crystallinity. The substitution of energy sources, *e.g.* microwaves and plasma, can accelerate the reaction rate and acquire a high yield of 3D COFs at relatively

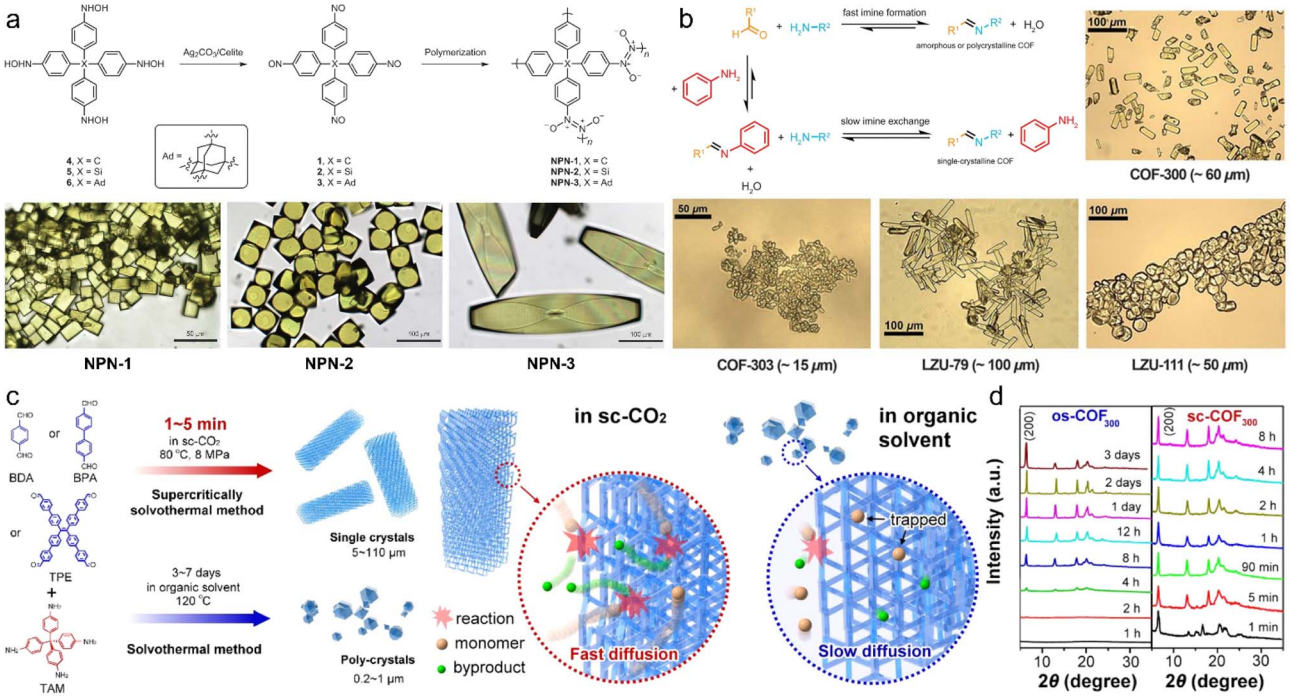

Fig. 4 (a) Synthesis scheme of NPN-1, NPN-2, and NPN-3, and corresponding photographs. Reproduced with permission.[77] Copyright 2013, Springer Nature. (b) Crystal growth of imine-based COFs with aniline as a modulator and photographs of COF-300, COF-303, LZU-79, and LZU-111. Reproduced with permission.[31] Copyright 2018, American Association for the Advancement of Science. (c) Schematic illustration of synthesis and crystal growth of 3D COFs in sc-CO_2 and organic solvent. (d) PXRD patterns of 3D COFs grown in sc-CO_2 and organic solvent at different times. Reproduced with permission.[80] Copyright 2022, American Chemical Society.

low temperatures, but there are few reports on microwave-assisted synthesis and plasma-induced synthesis. The use of green solvents, *e.g.* ILs and DES, provides an alternative avenue for the environmentally friendly synthesis of 3D COFs in a short time and on a large scale, but it is also limited to the rare successful samples of ionothermal synthesis and DES-assisted synthesis. The limitations of the synthetic methods are more prominent in the synthesis of single-crystal 3D COFs, which are only applicable to specific linkages. Although the structure of 3D COFs determined by SCXRD has been reported, the vast majority of obtained 3D COFs are microcrystalline and only allow for structure resolution with the aid of RED.

Until now, great efforts have been devoted to the synthesis of 3D COFs and several methods have been developed to facilitate their crystallization, whether in the form of powders or single crystals. Nevertheless, there are still very limited structures of 3D COFs, and it remains a huge challenge to prepare highly crystalline 3D COFs, in general, by convenient and effective methods.

Applications

With unique characteristics such as light element composition, periodic regular channels, designable and controllable structures, and high specific surface areas, 3D COFs have been widely used in gas storage and separation, catalysis, fluorescence, batteries, conductivity, drug delivery, and other fields.

Gas storage

In 2009, Yaghi *et al.* initiated the gas adsorption research of 3D COFs, demonstrating the well-performed uptake capacities for hydrogen (H_2), methane (CH_4), and carbon dioxide (CO_2), compared with 2D COFs, metal–organic frameworks, and other porous materials.[81] Subsequently, many reports on the gas storage performance of 3D COFs appeared.

For H_2 storage, Froudakis *et al.* replaced the phenylene moieties in COF-102 with diphenyl, triphenyl, naphthalene, and pyrene moieties to obtain COF-102-2, COF-102-3, COF-102-4, and COF-102-5, respectively and investigated their H_2 storage capacities by grand canonical Monte Carlo (GCMC) simulations.[82] Compared with COF-102, the optimized structure exhibited higher performance at both 77 and 300 K. COF-102-3 showed the highest H_2 storage, reaching 26.7 and 6.5 wt% at 100 bar, 77 and 300 K, respectively, exceeding the target proposed by the Department of Energy (DOE) (6 wt%) even at room temperature. He *et al.* reported the construction of 3D-*ceq*-COF and 3D-*hea*-COF using 2,3,6,7,14,15-hexa(4-formylphenyl) triptycene (HFPTP) with D_{3h} symmetry linked by 1,3,5-tris(4-aminophenyl)triazine (TAPT) with C_3 symmetry and tetrakis(4-aminobiphenyl)methane (TABPM) T_d symmetry.[58,59] High H_2 uptakes of 1.57 and 1.73 wt% at 77 K and 1 bar were observed for 3D-*ceq*-COF and 3D-*hea*-COF, respectively (Fig. 5a). Fang *et al.* functionalized the above D_{3h} and T_d monomers with fluorine groups to generate JUC-596 with a non-interpenetrated *hea* topology, which exhibited an enhanced H_2 uptake of

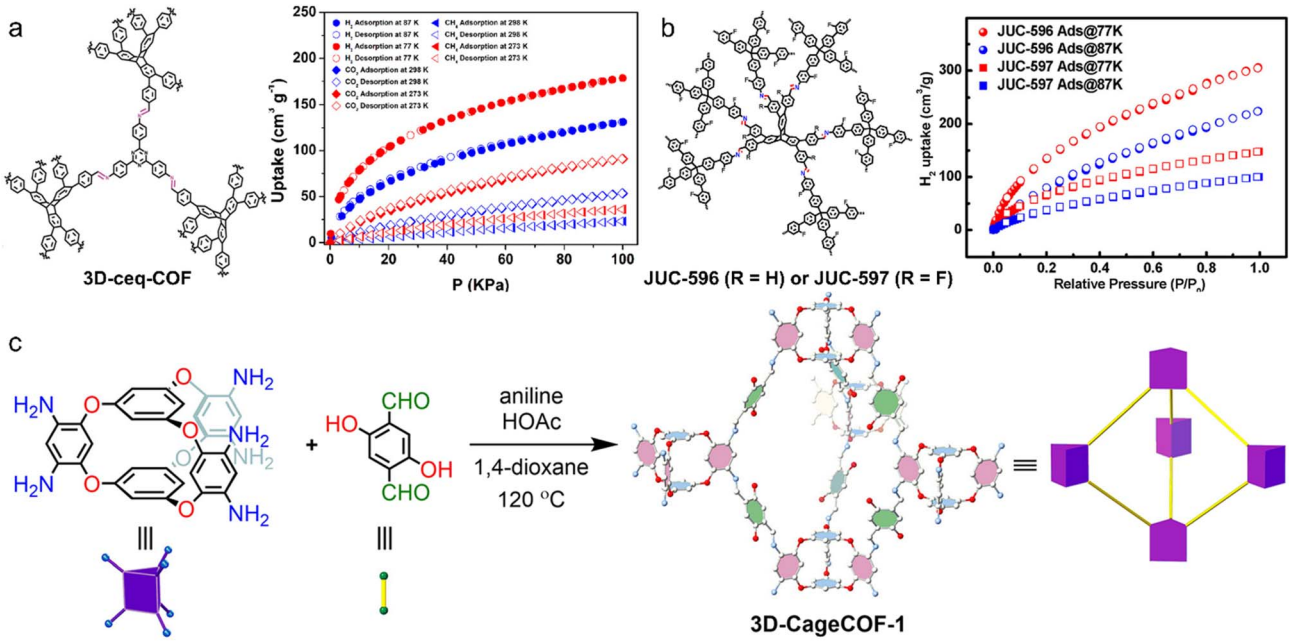

Fig. 5 (a) Schematic representation of 3D-*ceq*-COF and adsorption–desorption isotherms of H_2, CH_4, and CO_2. Reproduced with permission.[58] Copyright 2020, American Chemical Society. (b) Schematic representation of JUC-596 and JUC-597, and H_2 adsorption isotherms. Reproduced with permission.[83] Copyright 2022, Wiley-VCH GmbH. (c) Synthesis scheme of 3D-CageCOF-1. Reproduced with permission.[35] Copyright 2020, American Chemical Society.

2.72 wt% at 77 K and 1 bar, indicating the important role of triptycene in binding H_2 (Fig. 5b).[83]

For CH_4 storage, corresponding studies are relatively limited and mainly concentrated on the GCMC simulations. Cao *et al.* proposed a Li-doping method to improve CH_4 storage *via* the London dispersion and the induced dipole interaction because of the strong affinity between Li^+ and CH_4.[84] At 298 K and 35 bar, the CH_4 uptakes of Li-doped COF-102 and COF-103 reached 303 and 290 v(STP)/v, respectively, which are more than twice those of the original materials (127 and 108 v(STP)/v). Goddard *et al.* reported another approach of modification with alkyl substituents.[85] CH_4 delivery amounts of designed COF-103-Eth-trans and COF-102-Ant reached 192 and 180 v(STP)/v, respectively, exceeding the DOE target of 180 v(STP)/v at 35 bar. Smit *et al.* assembled a database of 69 840 novel COFs consisting of 666 different organic ligands and 4 synthesis routes *in silico*.[86] It turns out that the optimal structure consists of a carbon–carbon bond triazine linker with *tbd* topology, and shows a predicted delivery capacity of 216 v(STP)/v at 65 bar. Furthermore, it is predicted that *qzd*, *pth*, and *pts* topologies are generally the best for CH_4 storage in C–N bonding structures, while *ukk*, *uon*, and *dia* are the most common for C–C bonding structures.

For CO_2 capture, the introduction of various binding sites has been demonstrated to be an effective strategy. Fang *et al.* for the first time trapped [BMIm][NTf_2] in 3D-IL-COFs to enhance CO_2 uptake *via* the interaction between CO_2 and IL.[75] Wang *et al.* introduced azine bonds to 3D-HNU5, which exhibited a CO_2 adsorption capacity of 123.1 mg g^{-1} at 273 K.[87] Cooper *et al.* reported 3D-CageCOF-1 with abundant O and N atoms, creating a polar and hydrophilic environment favourable for CO_2 (Fig. 5c).[35] The maximum uptakes at 1 bar are 204 and 107 mg g^{-1} at 273 and 298 K, respectively.

As the major radioactive vapor waste in fission, iodine (I_2) capture has aroused great interest in recent years. Jiang *et al.* synthesized COF-DL229 using an adamantane monomer with T_d symmetry and implemented it to remove I_2 vapor.[88] COF-DL229 exhibited a high uptake capacity of 4.7 g g^{-1} (82.4 wt%) at 348 K and ambient pressure and maintained good performance (2.3 g g^{-1}, 70 wt%) even under ambient conditions. The introduction of functional groups is beneficial for performance improvement. Zhao *et al.* reported that CPOF-2 and CPOF-3 functionalized with electron-rich acetylene and diacetylene groups exhibited high adsorption capacities of 5.40 and 5.87 g g^{-1}, respectively.[89] Fang *et al.* also demonstrated a strong interaction between tetrathiafulvalene (TTF) and I_2 in JUC-561 with an excellent uptake of 8.19 g g^{-1}.[90]

Gas separation

Customized pore sizes, interconnected nanochannels, and high structural robustness of 3D COFs are beneficial for gas separation applications. As mentioned above, 3D COFs exhibit good affinity for CO_2 by introducing various binding sites, which can be applied to CO_2/N_2 and CO_2/CH_4 separation. For example, high CO_2/N_2 and CO_2/CH_4 selectivities of 24.6 and 23.1 in 3D-IL-COF-1, 24.0 and 22.3 in 3D-IL-COF-2, and 24.4 and 21.5 in 3D-IL-COF-3 were observed.[75]

In addition, there are some reports on the separation of light hydrocarbons. Zhang *et al.* reported a bottom-up [8 + 2] approach for the direct construction of 8-connected 3D COFs *via* 4′,5′-bis(3,5-diformylphenyl)-3′,6′-dimethyl-[1,1′:2′,1″-terphenyl]-

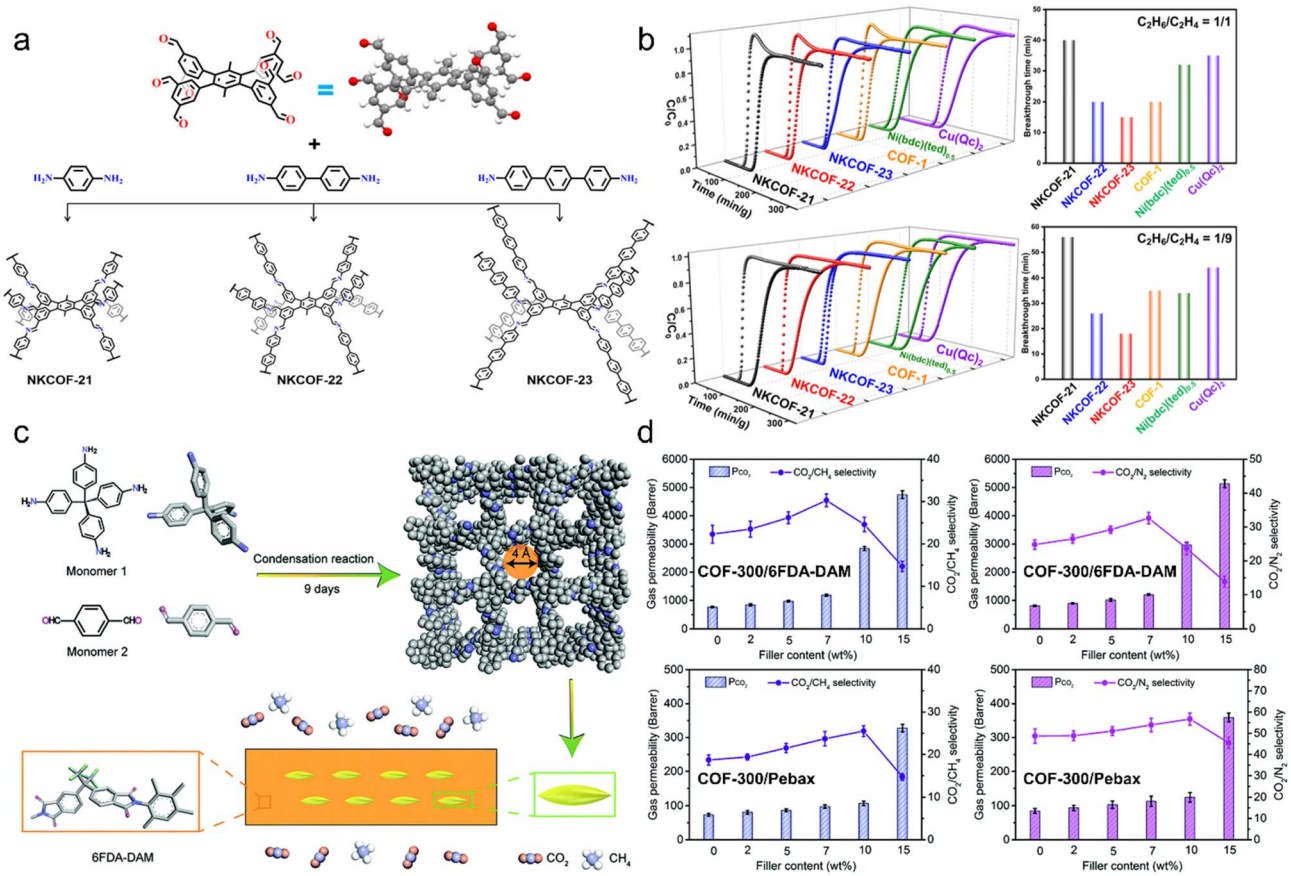

Fig. 6 (a) Synthetic procedures of NKCOF-21, -22, and -23. (b) Dynamic breakthrough curves and breakthrough time intervals for different adsorbents at 298 K and 1 bar. Reproduced with permission.[91] Copyright 2022, American Chemical Society. (c) Schematic illustration of COF-300/6FDA-DAM-MMM for CO_2/CH_4 separation. (d) Membrane separation performance tested under ambient conditions. Reproduced with permission.[92] Copyright 2019, Royal Society of Chemistry.

3,3″,5,5″-tetracarbaldehyde (DPTB-Me) with D_{2h} symmetry (Fig. 6a).[91] The obtained NKCOF-21, -22, and -23 all exhibited preferential adsorption of ethane (C_2H_6) over ethylene (C_2H_4) due to the nonpolar pore environment. Among them, NKCOF-21 with the optimal performance demonstrated differential uptakes of 97.9 and 74.3 $cm^3\ g^{-1}$ for C_2H_6 and C_2H_4, respectively. Dynamic breakthrough experiments indicated that C_2H_6/C_2H_4 (1/1 and 1/9) mixtures could be effectively separated to obtain high-purity C_2H_4 (>99.99%) with a productivity of 6.8 L kg^{-1} (Fig. 6b). Subsequently, they achieved efficient removal of trace propyne (C_3H_4) to obtain high-purity propylene (C_3H_6) from a C_3H_4/C_3H_6 (1/99 and 0.1/99.9) mixture, using NKCOF-36 and NKCOF-37 based on DPTB-Me and two tetratopic monomers with T_d symmetry.[62]

Membrane separation is also a research hotspot in 3D COFs. Gao *et al.* first reported a COF-320 membrane grown on α-Al_2O_3 substrate modified using 3-aminopropyltriethoxysilane (APTES).[93] The obtained 3D COF-320 membrane exhibited a higher H_2 permeance of 5.67×10^{-7} mol ($m^{-2}\ s^{-1}\ Pa^{-1}$) compared to CH_4 and N_2, and a permselectivity of 2.5 and 3.5 was observed for H_2/CH_4 and H_2/N_2, respectively. Zhao *et al.* added COF-300 into two polymer matrixes, 6FDA-DAM and Pebax, and demonstrated the potential of 3D COFs for CO_2 capture in a mixed matrix membrane (MMM) (Fig. 6c).[92] The results indicated that porous COF-300 increased the free volume fraction of the membrane and thus enhanced its permeability (Fig. 5d). Meanwhile, the narrow pores of COF-300 and the rigid polymer chains on the surface enhance the size discrimination process, thereby improving its selectivity.

Catalysis

As promising platforms for catalysis, 3D COFs possess abundant active sites that are accurately anchored to the channel through *in situ*, pre- or post-modification. The insolubility and high stability of 3D COFs confirmed their heterogeneous nature and good reusability.[94] In recent years, photocatalysis and electrocatalysis have attracted increasing attention in 3D COFs.

Porphyrins are common photoactive sites in 3D COFs.[95] Zhang *et al.* reported NUST-5 and NUST-6 constructed from 5,10,15,20-tetrayl(tetrakis([1,1′:3′,1″-terphenyl]-4,4′′-dicarbaldehyde))-porphyrin (TTEP) for photocatalytic CO_2 reduction (Fig. 7a).[50] After visible light irradiation for 10 h, NUST-5 and NUST-6 exhibited a high CO production of 54.7 and 76.2 μmol g^{-1}, respectively, but a relatively low CH_4 yield of 17.2 and 12.8 μmol g^{-1}, respectively. The CO/CH_4 production ratios were 76% and 86%, indicating their high photocatalytic

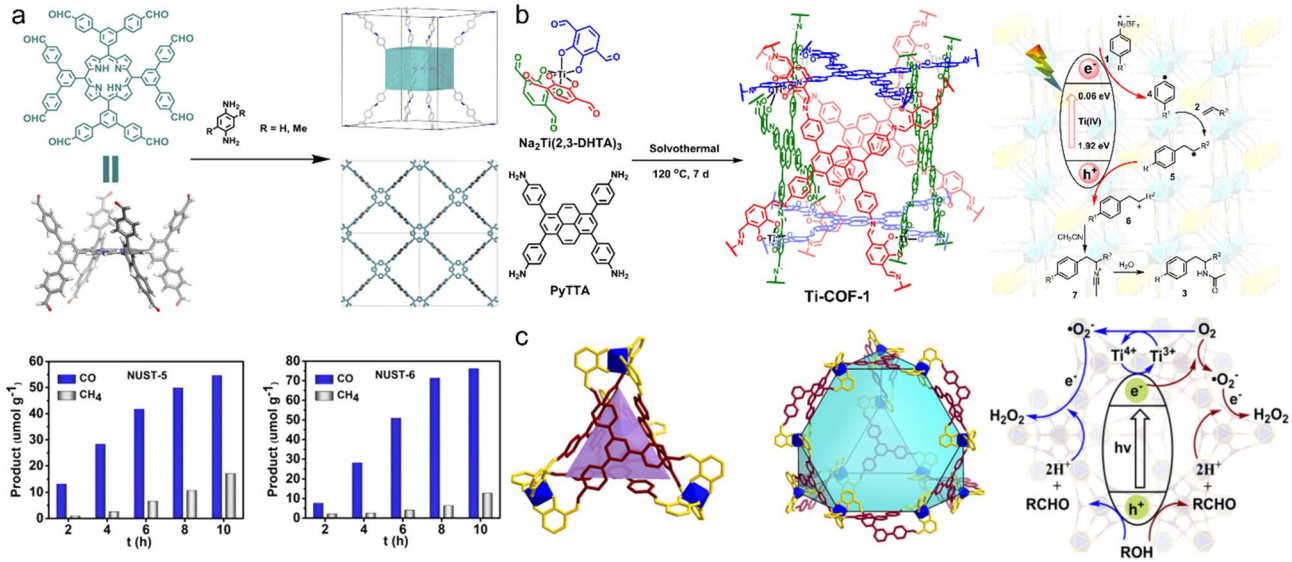

Fig. 7 (a) Synthetic illustration of NUST-5 and NUST-6 and photocatalytic production of CO and CH_4. Reproduced with permission.[50] Copyright 2022, American Chemical Society. (b) Synthetic illustration of Ti-COF-1 and the proposed mechanism of the photocatalytic Meerwein addition reaction. Reproduced with permission.[61] Copyright 2021, Wiley-VCH GmbH. (c) The tetrahedral cage and truncated tetrahedral cage in TiCOF-*spn*, and the proposed mechanism of photocatalytic H_2O_2 production. Reproduced with permission.[65] Copyright 2022, Elsevier.

selectivity. In the same year, Huang *et al.* constructed TAPP-HFPB-COF with 5,10,15,20-tetra(4-aminophenyl)porphyrin (TAPP) for the photocatalytic α-functionalization of aldehydes and CO_2 reduction.[64] After 6 h, a better CO/CH_4 selectivity of 96% was observed with a differential production of 128 and 5 μmol g^{-1} for CO and CH_4, respectively.

Introducing photoactive metal centers into 3D COFs has proven to be another effective strategy for the design of photocatalysts. Gu *et al.* designed a Ti(IV) complex, $Na_2Ti(2,3\text{-}DHTA)_3$ (2,3-DHTA = 2,3-dihydroxyterephthalaldehyde), with C_3 symmetry as a building block for the synthesis of anionic Ti-COF-1 (Fig. 7b).[61] The wide absorption band in the ultraviolet//visible (UV/vis) spectrum and an optical energy gap of 1.86 eV endow Ti-COF-1 with high photocatalytic activity for the Meerwein addition reaction, which is a valuable method for the industrial synthetic process of drugs and fine chemicals. It was found that Meerwein addition reactions catalyzed by Ti-COF-1 can tolerate various arenediazonium salts and alkenes to obtain desired products with a yield of 49–75% and turnover number (TON) of 132–202. After substitution of 4,4′,4″,4‴-(pyrene-1,3,6,8-tetrayl)tetraaniline (PyTTA) in Ti-COF-1 with 1,3,5-tris(4-aminophenyl) triazine (TAPT), TiCOF-*spn* with strong absorption of visible light and efficient photocatalytic production of hydrogen peroxide (H_2O_2) was reported (Fig. 7c).[65] In a pure water system, the H_2O_2 yield was 223.55 μmol (g^{-1} h^{-1}), while in a water/ethanol system, when the ratio was changed from 9/1 to 1/9, the H_2O_2 yield increased significantly from 280.33 μmol (g^{-1} h^{-1}) to 489.94 μmol (g^{-1} h^{-1}).

As electroactive sites, the introduction of porphyrin and phthalocyanine (Pc) to 3D COFs enables outstanding electrocatalytic performance. Huang *et al.* synthesized 3D-Por(Co/H)-COF with mixed monomers of TAPP and its cobalt derivative Co-TAPP, exhibiting high activity towards the CO_2 reduction reaction (CO_2RR) with a CO faradaic efficiency of 92.4% at −0.6 V.[96] Jiang *et al.* reported CoPc-PI-COF-3 (PI = polyimide) doped with carbon black as an electrocatalytic cathode, exhibiting a high CO faradaic efficiency of 96% at −0.9 V.[97] The porous structure of CoPc-PI-COF-3 results in the proportion of active electrocatalytic centers reaching 32.7% of the cobalt phthalocyanine subunits, affording a high current density of −31.7 mA cm^{-2} at −0.9 V.

The linkages in 3D COFs can also serve as catalytic centers, particularly acid/base sites. Imine linkages are commonly observed in 3D COFs and can act as basic catalysis active sites due to their basicity. For example, Yan *et al.* reported the intrinsic basic catalytic performance of imine-linked BF-COF-1 and BF-COF-2 for Knoevenagel condensation reactions.[98] Both BF-COFs showed significant conversions (96% for BF-COF-1 and 98% for BF-COF-2) and high size selectivity, indicating that the reaction occurred within the pores of BF-COFs. Similarly, boroxine linkage with acidity can act as an acidic catalytically active site. Qiu *et al.* designed two DL-COFs with dual linkages of boroxine and imine for acidic and basic one-pot cascade catalytic reactions.[99] The cascade reactions involve acetal hydrolysis catalyzed by the acidic site of the boroxine ring, followed by Knoevenagel condensation catalyzed by the alkaline site of the imine group. DL-COFs can be easily separated from the reaction mixture and reused at least three times with little loss of activity by simple filtration.

Generally, there are two main strategies to tune the catalytic activity of COFs, pre-functionalization and post-functionalization, both of which are irreversible and complicated. As an alternative, supramolecular functionalization appears to be a facile approach for the regulation of catalytic activity. Alemán *et al.* conducted reversible supramolecular functionalization in COF-300 with a carboxylic acid (acetic acid)

for catalyzing ring-opening reactions of epoxides and a Brønsted base (triethylamine) for catalyzing Knoevenagel condensation, respectively.[100] This work provides new options to regulate the catalytic performance of COFs *via* non-covalent encapsulation of acidic or alkaline small molecules.

Fluorescence

3D COFs with uniform channels modified by fluorophores are promising candidates for fluorescence emission and sensing. Wang *et al.* reported the first fluorescent pyrene-based 3D-Py-COF with intense yellow-green emission, due to the presence of isolated pyrene moieties, which initiated the research on 3D COFs in fluorescence applications.[54] Subsequently, they introduced tetraphenylethylene (TPE), one of the representative aggregation-induced emission luminogens (AIEgens), into 3D-TPE-COF displaying yellow fluorescence emission with a quantum yield of 20%.[101] After facile coating on commercial blue light emitting diodes (LEDs), white LEDs were fabricated and exhibited no degradation under continuous driving for 1200 h.

To date, most research has focused on internal changes in absorption and luminescence characteristics, while rarely involving external stimuli, whether physical stimuli such as mechanical force, light, heat, electricity, and magnetism or chemical stimuli such as pH, moisture, and chemicals. Fang *et al.* for the first time investigated piezochromism in 3D COFs under mechanical stimuli with the diamond anvil cell technique (Fig. 8a).[102] They linked electron-donating triphenylamine (TPA) with electron-deficient benzimidazole (BI) for the synthesis of a donor–acceptor (D–A) conjugated TPA-BI, and selected a benzisothiadiazole derivative (BTD) without TPA for comparison. JUC-635 constructed from TPA-BI exhibited twisted intramolecular charge transfer (TICT) and AIE, while JUC-635 constructed from BTD exhibited aggregation-caused quenching (ACQ). In contrast to the continuous fluorescence decrease with increasing pressure in JUC-636 (Fig. 8c), the fluorescence was maintained up to 3 GPa in JUC-635 and reversible piezofluorochromism with a high-contrast emission difference of 187 nm was observed at 12 GPa (Fig. 8b).

Furthermore, fluorescence sensing of ions is another application of 3D COFs. Shi *et al.* reported stable COF-TT composed of a bis(tetraoxacalix[2]arene[2]triazine) core and applied it as a turn-off fluorescent sensor for Fe^{3+} cations and CrO_4^{2-}, $Cr_2O_7^{2-}$, and MnO_4^- anions.[104] Qiu *et al.* synthesized hydroxyl-functionalized TAPM-DHBD realizing reversible uranium (UO_2^{2+}) detection and extraction simultaneously (Fig. 7d).[103] TAPM-DHBD exhibited a rapid response time of 2 s, a detection limit of 4.08 nM, an excellent uranium extraction capacity of 955.3 mg g^{-1} and fast kinetics, indicating its potential for sensitive and on-site monitoring of radioactive uranium contamination.

Batteries

The highly ordered mass transport channels, rigid long-range conjugation system, and uniform porous framework endow 3D COFs with potential applications as electrodes for energy storage, such as lithium-ion batteries (LIBs), lithium–sulfur batteries (LSBs), and zinc–air batteries (ZABs).

Based on the spirobifluorene core, Huang *et al.* reported the self-templated synthesis of uniform hollow spheres of conjugated 3D-Sp-COF, and utilized it as an electrode in LIBs.[105] 3D-Sp-COF exhibited good lithium ion transport performance with a transference number of 0.7 and a high specific capacitance of 251 F g^{-1} at 0.5 A g^{-1}. Notably, due to the wetting activation of the hollow spheres, the specific capacitance increases sharply with the increasing cycle numbers, reaching a maximum of 364

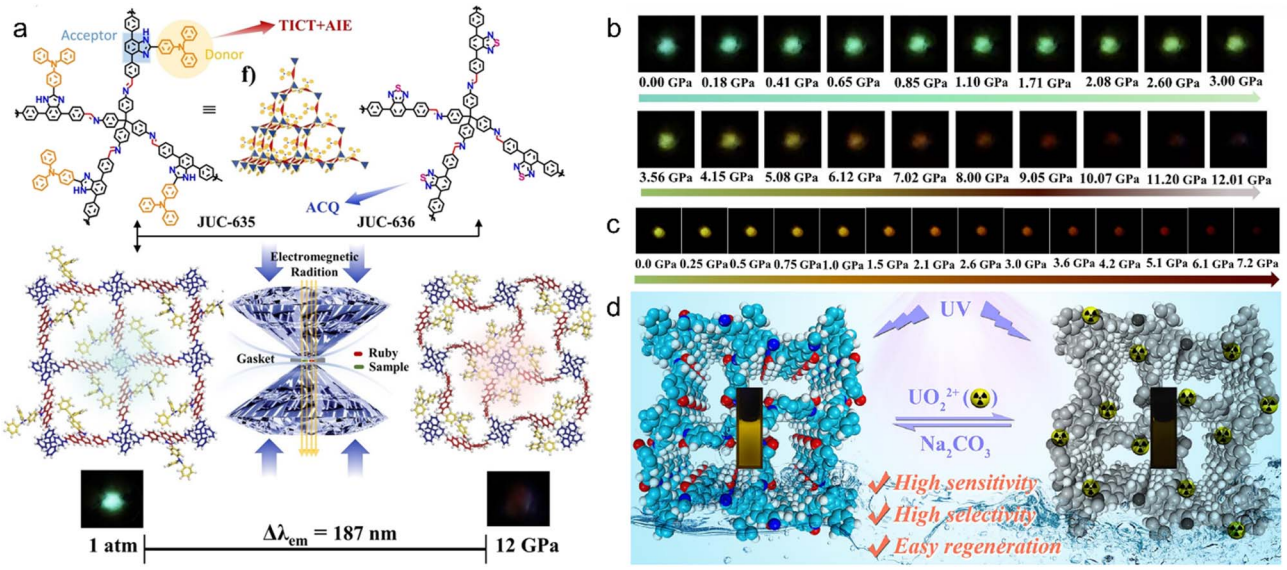

Fig. 8 (a) Schematic representation of JUC-635 and JUC-636, and the piezochromic behavior. Photographs of (b) JUC-635 and (c) JUC-636 at various pressures. Reproduced with permission.[102] Copyright 2023, Wiley-VCH GmbH. (d) Illustration of TAPM-DHBD for reversible uranium detection and extraction. Reproduced with permission.[103] Copyright 2022, Elsevier.

F g^{-1} at 3 A g^{-1}. Jiang *et al.* constructed conjugated 3D-*scu*-COF-1 and 3D-*scu*-COF-2 *via* the condensation of 6,13-dimethoxy-2,3,9,10,18,19,24,25-octa(4′-formylphenyl)pentiptycene (DMOPTP) and two square-planar monomers (Fig. 9a).[49] The conjugation properties enabled π–electron delocalization in both structures, displaying high conductivities of 3.2 and 3.5 × 10^{-5} S cm^{-1} for 3D-*scu*-COF-1 and 3D-*scu*-COF-2, respectively. After introducing sulfur *via* melt infiltration, they were both applied as electrodes in LSBs with excellent capacities of 1035 and 1155 mA h g^{-1} at 0.2C, high rate capabilities of 713 and 757 mA h g^{-1} at 5.0C, and outstanding cycling stabilities of 71% and 83% capacity retention at 2.0C after 500 cycles for 3D-*scu*-COF-1 and 3D-*scu*-COF-2, respectively (Fig. 9b).

Currently reported 3D COFs are usually powders, which require further processing before they can be used as electrodes. Thus, the direct synthesis of 3D COF thin films on electrodes is crucial for the practical application of devices. Liang *et al.* proposed *in situ* solvent-free synthesis of 3D COF thin films *via* thermal evaporation and deposition of 1,3,5-triformylphloroglucinol (Tp) and 4,4′-biphenyldicarboxaldehyde (BPDA) with tetrakis(4-aminophenyl)methane (TAM) on Zn plates (Fig. 9c).[106] Compared with TAM-BPDA thin films, TAM-Tp thin films exhibited excellent hydroxide ion transport capacity (85.3 mS cm^{-1}) and significant inhibition on Zn dendrites, with a power density of 63.8 mW cm^{-2} and cycle life of 58 h in quasi-solid state TAM-Tp-based ZABs, and a higher power density of 111.6 mW cm^{-2} and longer cycle life of 600 h in aqueous TAM-Tp-based ZABs. Quasi-solid state TAM-Tp-based ZABs maintained stable work at bending angles of 0°, 60°, 120°, and 180°, and the series connection of two ZABs could light up a small LED bulb (1.7 V, 20 mA) and a LED screen (1.5 V, 100 mA), indicating their practical application in energy devices (Fig. 9d).

Conductivity

3D COFs also exhibit good ionic or electric conductivity owing to the presence of interpenetrated channels, conjugated skeletons, and accessible functional moieties. Counterions can serve as carriers in 3D COFs to modulate the ionic conductivity. For instance, Feng *et al.* constructed anionic CD-COFs with flexible aliphatic γ-cyclodextrin (γ-CD) and tetrakis(spiroborate) tetrahedra with different counterions.[55] The flexibility of γ-CD endows CD-COFs with dynamic characteristics and a high Li^+ ion conductivity of 2.7 mS cm^{-1} for the charged skeleton and a high capability to intercept electrolytes in restricted channels. Perepichka *et al.* reported the reversible transformation between vinylene-linked 2D COFs and cyclobutane-linked 3D COFs.[107] After being impregnated with $LiClO_4$, the 3D COFs showed a significant Li^+ ion conductivity of 3.5 × 10^{-5} S cm^{-1}, and a higher proton conductivity of 2.2 × 10^{-3} S cm^{-1} after being treated with H_2SO_4 at room temperature.

Chemical doping is an effective method to improve electric conductivity by forming charge transfer complexes, and I_2 is a frequently used dopant. Fang *et al.* discovered the tuneable electrochemical activity of 3D-TTF-COFs due to redox active TTF moieties that form organic salts.[108] As I_2 doping increases, the electric conductivity can be tuned from 1.8 × 10^{-7} to 1.4 × 10^{-2} S cm^{-1}. Recently, Chen *et al.* also reported a significant enhancement of over 6 orders of magnitude in electric conductivity after doping with I_2 in DDHP-COF.[67] The charge transfer between I_2 molecules and DDHP-COF to form positively

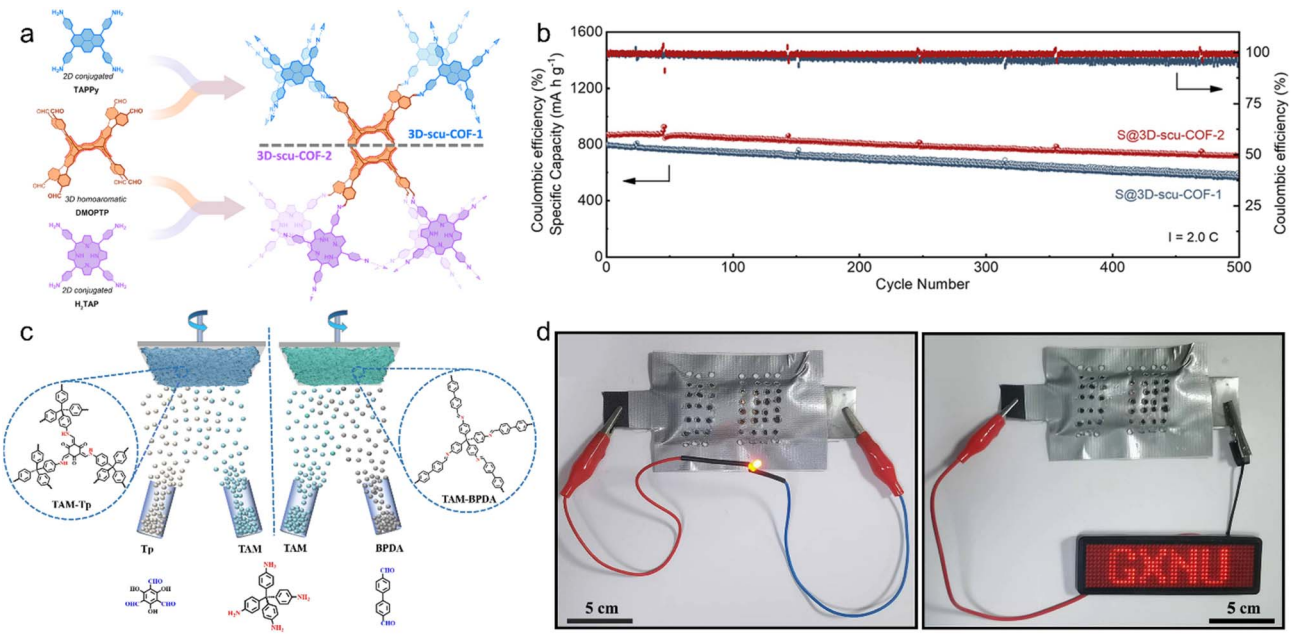

Fig. 9 (a) Synthetic illustration of 3D-*scu*-COF-1 and 3D-*scu*-COF-2. (b) Cycling stability of S@3D-*scu*-COF-1 and S@3D-*scu*-COF-2 electrodes at 2.0C. Reproduced with permission.[49] Copyright 2022, American Chemical Society. (c) Schematic illustration for the synthesis of TAM-Tp and TAM-BPDA thin films. (d) Photographs of LEDs lit using two series-connected TAM-Tp-based quasi-solid state ZABs. Reproduced with permission.[106] Copyright 2023, Elsevier.

charged free radicals and negatively charged iodide counterions may explain the reason for the great enhancement.

Understanding thermal properties is the foundation for energy conservation and sustainable development. The low density and interlaced voids also enable 3D COFs to be a candidate for thermal conductivity, but only a few studies have been reported. Feng *et al.* predicted the thermal conductivities of four boron-based 3D COFs on the order of 0.1 W (m^{-1} K^{-1}) at 300 K with molecular dynamics (MD) simulations using the Green–Kubo method.[109] As the temperature increased from 200 K to 500 K, the thermal conductivity decreased by 47%, indicating its temperature dependence. Subsequently, Esteves *et al.* measured the thermal conductivity of COF-300, RIO-1, and RIO-4 with the modified transient plane source (MTPS) technique, ranging from 0.038 to 0.048 W (m^{-1} K^{-1}) at 298 K.[110] The results also indicated a linear relationship between thermal conductivity and the reciprocal of pore cross-sectional area. However, the potential of ultra-high thermal conductivity still needs to be further explored due to the high crystallinity and adjustable pore size of 3D COFs. Tian *et al.* observed an ultra-high thermal conductivity of over 15 W (m^{-1} K^{-1}) in COF-300 derivatives at a pore size of 0.63 nm with MD simulations.[111] Further calculations of temperature-dependent thermal conductivity and XRD patterns emphasized that maintaining microscopic order is important to achieve high thermal conductivity.

Drug delivery

In order to overcome the limitations of effective drug delivery to cells and tissues, such as non-targeted accumulation and multidrug resistance, significant efforts have been devoted to developing drug carriers for efficient and non-toxic drug delivery systems. In recent years, 3D COFs with low cytotoxicity due to the absence of metal elements have attracted great attention since Yan *et al.* initiated the research on 3D COFs for drug delivery in 2015.[112] They reported two 3D PI-COFs with suitable pore sizes to entrap ibuprofen (IBU), a widely used non-steroidal anti-inflammatory drug for the treatment of inflammation, pain, and rheumatism. The release curves of 3D PI-COFs loaded with IBU revealed that PI-COF-4 and PI-COF-5 released 60% and 49% of the drug after 12 h, respectively, while the complete release took up to 6 days for both cases. PI-COF-5 with smaller pore size and a 4-fold interpenetrated structure exhibited a lower release rate than PI-COF-4 with larger pore size and a non-interpenetrated structure, confirming that the drug release depended on their geometry and pore aperture.

Recently, Negishi *et al.* constructed TUS-84 with novel *scu* topology exhibiting efficient loading and sustained release of IBU.[63] A slow release rate of 24% was observed after 12 h, indicating the long-acting formulation and sustained concentration of IBU for a long time. This could reduce the dosing frequency and ensure more consistent control of long-term pain. Subsequently, they reported TUS-64 with a record ultra-large pore of 47 Å and ultra-low density of 0.106 g cm^{-3}, exhibiting effective drug loading and controlled release of five different drugs in a simulated body fluid environment.[113] Remarkably, TUS-64 showed a high loading of 17.34 wt% for anticancer drug 5-fluorouracil and a sustained release rate of about 12% after 9 days.

In addition to drug release at pH = 7.4 to simulate normal body fluids, the performance at pH = 4.8 to simulate cancer fluid matters for cancer therapeutics. Fang *et al.* unveiled the first stimuli-responsive drug delivery system using 3D hydrazone-functionalized COFs as pH-triggered rotary switches.[114] The construction was based on pH-responsive ethyl-2-(2-(4,4″-diaminobiphenyl)hydrazono)-2-(pyridin-2-yl)acetate (HZ) with *E*/*Z* interconversion. As a traditional drug for cancer treatment, especially for pancreatic cancer, acute myelogenous leukemia and chronic lymphoma, cytarabine (Ara-C) was chosen as the model molecule loaded in JUC-556-$[HZ]_X$ and its pH-responsive release was investigated. The drug release at pH = 4.8 has increased by nearly four times compared to that at pH = 7.4, which effectively improved drug targeting and reduced side effects.

Summary and outlook

Featuring low density, high specific surface areas, uniformly ordered channels, designable structures, and assessable active moieties, 3D COFs are promising application platforms and have attracted great interest. Compared to 2D COFs with layered structures stacked *via* non-covalent interactions, *e.g.* π–π stacking, van der Waals interactions, and hydrogen bonds, 3D COFs with the entire covalent connection usually have the upper hand in practical applications due to their interconnected channels, hierarchical nanopores, and facilely available active sites. Although current research mainly focuses on 2D COFs, the excellent performance of 3D COFs endows them with enormous potential in a wide range of application fields. In this review, we briefly summarized the development process of 3D COFs from the perspective of reported topologies and synthetic methods and discussed their recent progress in multifunctional applications, such as gas storage and separation, catalysis, fluorescence, batteries, conductivity, and drug delivery.

Nevertheless, there are still huge challenges to be solved during the development of 3D COFs. One of the major problems to be addressed is the crystallization of 3D COFs in the absence of a driving force, *e.g.* strong π–π stacking, compared with 2D COFs. Therefore, the preparation of 3D COFs requires precise adjustments. 3D COFs are generally synthesized under solvothermal conditions with plenty of parameters affecting structures, such as solvents, catalysts, and temperature. Many other strategies used for the synthesis of crystalline porous materials, such as mechanochemical synthesis, electrochemical synthesis, dry-gel conversion synthesis, interfacial synthesis, continuous flow synthesis, and high-throughput synthesis, are still waiting to be explored in 3D COFs, especially the obtainment of high-quality single crystals, which is another bottleneck in the identification of 3D COF structures. The study of the growth mechanism of 3D COFs is still important and may make breakthroughs as the synthetic methods gradually mature, thereby facilitating strategies to obtain 3D COFs with high crystallinity. Another technical hurdle is extending research

from purely fundamental characteristics to more practical properties, such as mechanical, chemical, and long-term environmental stability, in order to gain a deeper understanding of the operational scope of 3D COFs. Great efforts should be devoted to the development of effective synthetic methods to acquire target structures without by-products. To further satisfy the industrial requirements, green synthesis conditions should be considered, *e.g.* cheap and non-toxic chemicals, non-flammable, non-corrosive, and recyclable reaction media, cost-effective and reliable energy sources, *etc.*

Currently, the application of 3D COFs is still restricted by the lack of various structures due to the limited availability of building blocks. Rational design of new monomers and linkages under the guidance of reticular chemistry for discovering new topologies can enrich the structural diversity of 3D COFs, further broadening the application fields. Functionalization *via* active linkages, predesigned building blocks, and post-synthesis is another important method to improve performance, but there are also issues to be addressed, such as few options for active linkages, crystallization problems after introducing functional groups, and damage to crystals during post-synthesis. Meanwhile, 3D COF membranes and thin films provide another avenue for practical applications. The establishment of structure–property relationships in 3D COFs with the aid of theoretical calculations is also an essential development direction, which can provide guidance for the modularized and customized design of specific function-oriented 3D COFs. For 3D COFs with practical application prospects, further improving performance to meet industrial requirements and developing suitable processing and shaping methods are essential technical obstacles that need to be overcome. In addition, large-scale manufacturing with high space-time yield is also an inevitable issue to be solved in practical application.

As an emerging functional porous material, 3D COFs demonstrate broad application prospects and huge challenges, and great efforts need to be continuously devoted to this promising research hotspot. We hope that this review can provide potential guidance for the rational design and synthesis of 3D COFs with novel topologies and practical applications.

Author contributions

Conceptualization, investigation, and writing-original draft: Xiaokang Wang; writing-review & editing: Fei Gao and Zixi Kang; supervision and funding acquisition: Weidong Fan and Daofeng Sun.

Conflicts of interest

There are no conflicts to declare.

Acknowledgements

This work was supported by the National Natural Science Foundation of China (NSFC, Grant No. 22275210, 22201305, and 22171288), the Fundamental Research Funds for the Central Universities (22CX06024A and 23CX04001A), and the Outstanding Youth Science Fund Projects of Shandong Province (2022HWYQ-070 and ZR2022YQ15).

References

1 R. Liu, K. T. Tan, Y. Gong, Y. Chen, Z. Li, S. Xie, T. He, Z. Lu, H. Yang and D. Jiang, *Chem. Soc. Rev.*, 2021, **50**, 120–242.
2 C. Wang, Z. Zhang, Y. Zhu, C. Yang, J. Wu and W. Hu, *Adv. Mater.*, 2022, **34**, e2102290.
3 R. Shevate and D. L. Shaffer, *ACS Nano*, 2022, **16**, 2407–2418.
4 Z. Wang, S. Zhang, Y. Chen, Z. Zhang and S. Ma, *Chem. Soc. Rev.*, 2020, **49**, 708–735.
5 H. Fan, M. Peng, I. Strauss, A. Mundstock, H. Meng and J. Caro, *Nat. Commun.*, 2021, **12**, 38.
6 X. Liang, H. Wu, H. Huang, X. Wang, M. Wang, H. Dou, G. He, Y. Ren, Y. Liu, Y. Wu, S. Wang, H. Ge, C. Zhong, Y. Chen and Z. Jiang, *J. Mater. Chem. A*, 2022, **10**, 5420–5429.
7 Y.-N. Gong, X. Guan and H.-L. Jiang, *Coord. Chem. Rev.*, 2023, **475**, 214889.
8 R. Chen, J. L. Shi, Y. Ma, G. Lin, X. Lang and C. Wang, *Angew. Chem., Int. Ed.*, 2019, **58**, 6430–6434.
9 J. Xu, C. Yang, S. Bi, W. Wang, Y. He, D. Wu, Q. Liang, X. Wang and F. Zhang, *Angew. Chem., Int. Ed.*, 2020, **59**, 23845–23853.
10 Y. Feng, Y. Xu, S. Liu, D. Wu, Z. Su, G. Chen, J. Liu and G. Li, *Coord. Chem. Rev.*, 2022, **459**, 214414.
11 M. Faheem, S. Aziz, X. Jing, T. Ma, J. Du, F. Sun, Y. Tian and G. Zhu, *J. Mater. Chem. A*, 2019, **7**, 27148–27155.
12 J.-Y. Yue, X.-L. Ding, Y.-T. Wang, Y.-X. Wen, P. Yang, Y. Ma and B. Tang, *J. Mater. Chem. A*, 2021, **9**, 26861–26866.
13 L. Kong, M. Liu, H. Huang, Y. Xu and X. H. Bu, *Adv. Energy Mater.*, 2021, **12**, 2100172.
14 C. Wu, Y. Liu, H. Liu, C. Duan, Q. Pan, J. Zhu, F. Hu, X. Ma, T. Jiu, Z. Li and Y. Zhao, *J. Am. Chem. Soc.*, 2018, **140**, 10016–10024.
15 R. Chen, J. Zhao, Z. Yu, M. Cong, Y. Wang, M. Wang, G. Li, Z. Li and Y. Zhao, *ACS Appl. Mater. Interfaces*, 2023, **15**, 830–837.
16 J. Lv, Y.-X. Tan, J. Xie, R. Yang, M. Yu, S. Sun, M.-D. Li, D. Yuan and Y. Wang, *Angew. Chem., Int. Ed.*, 2018, **57**, 12716–12720.
17 W. Liu, K. Wang, X. Zhan, Z. Liu, X. Yang, Y. Jin, B. Yu, L. Gong, H. Wang, D. Qi, D. Yuan and J. Jiang, *J. Am. Chem. Soc.*, 2023, **145**, 8141–8149.
18 C. Sun, D. Sheng, B. Wang and X. Feng, *Angew. Chem., Int. Ed.*, 2023, **62**, e202303378.
19 Z. Li, H. Li, X. Guan, J. Tang, Y. Yusran, Z. Li, M. Xue, Q. Fang, Y. Yan, V. Valtchev and S. Qiu, *J. Am. Chem. Soc.*, 2017, **139**, 17771–17774.
20 Q. Lu, Y. Ma, H. Li, X. Guan, Y. Yusran, M. Xue, Q. Fang, Y. Yan, S. Qiu and V. Valtchev, *Angew. Chem., Int. Ed.*, 2018, **57**, 6042–6048.
21 Y. Zhang, J. Guo, G. Han, Y. Bai, Q. Ge, J. Ma, C. H. Lau and L. Shao, *Sci. Adv.*, 2021, **7**, eabe8706.
22 X. Han, J. Huang, C. Yuan, Y. Liu and Y. Cui, *J. Am. Chem. Soc.*, 2018, **140**, 892–895.
23 Y. Chen, Z. L. Shi, L. Wei, B. Zhou, J. Tan, H. L. Zhou and Y. B. Zhang, *J. Am. Chem. Soc.*, 2019, **141**, 3298–3303.

24 J. Huang, X. Han, S. Yang, Y. Cao, C. Yuan, Y. Liu, J. Wang and Y. Cui, *J. Am. Chem. Soc.*, 2019, **141**, 8996–9003.
25 Y. Wang, C. Wu, W. Sun, Q. Pan, W. Hao, H. Liu, J. Sun, Z. Li, J. Sun and Y. Zhao, *Mater. Chem. Front.*, 2021, **5**, 944–949.
26 C. Ji, K. Su, W. Wang, J. Chang, E.-S. M. El-Sayed, L. Zhang and D. Yuan, *CCS Chem.*, 2022, **4**, 3095–3105.
27 Y. Li, W. Chen, G. Xing, D. Jiang and L. Chen, *Chem. Soc. Rev.*, 2020, **49**, 2852–2868.
28 Y. Mou, X. Wu, C. Qin, J. Chen, Y. Zhao, L. Jiang, C. Zhang, X. Yuan, E. Huixiang Ang and H. Wang, *Angew. Chem., Int. Ed.*, 2023, **62**, e202309480.
29 C. Qin, X. Wu, L. Tang, X. Chen, M. Li, Y. Mou, B. Su, S. Wang, C. Feng, J. Liu, X. Yuan, Y. Zhao and H. Wang, *Nat. Commun.*, 2023, **14**, 5238.
30 H. M. El-Kaderi, J. R. Hunt, J. L. Mendoza-Cortes, A. P. Cote, R. E. Taylor, M. O'Keeffe and O. M. Yaghi, *Science*, 2007, **316**, 268–272.
31 T. Ma, E. A. Kapustin, S. X. Yin, L. Liang, Z. Zhou, J. Niu, L. H. Li, Y. Wang, J. Su, J. Li, X. Wang, W. D. Wang, W. Wang, J. Sun and O. M. Yaghi, *Science*, 2018, **361**, 48–52.
32 Y. Xie, J. Li, C. Lin, B. Gui, C. Ji, D. Yuan, J. Sun and C. Wang, *J. Am. Chem. Soc.*, 2021, **143**, 7279–7284.
33 Y. Lan, X. Han, M. Tong, H. Huang, Q. Yang, D. Liu, X. Zhao and C. Zhong, *Nat. Commun.*, 2018, **9**, 5274.
34 X. Kang, X. Han, C. Yuan, C. Cheng, Y. Liu and Y. Cui, *J. Am. Chem. Soc.*, 2020, **142**, 16346–16356.
35 Q. Zhu, X. Wang, R. Clowes, P. Cui, L. Chen, M. A. Little and A. I. Cooper, *J. Am. Chem. Soc.*, 2020, **142**, 16842–16848.
36 C. Gropp, T. Ma, N. Hanikel and O. M. Yaghi, *Science*, 2020, **370**, eabd6406.
37 T. Sun, C. E. Hughes, L. Guo, L. Wei, K. D. M. Harris, Y. B. Zhang and Y. Ma, *Angew. Chem., Int. Ed.*, 2020, **59**, 22638–22644.
38 B. Gui, H. Ding, Y. Cheng, A. Mal and C. Wang, *Trends Chem.*, 2022, **4**, 437–450.
39 X. Guan, Q. Fang, Y. Yan and S. Qiu, *Acc. Chem. Res.*, 2022, **55**, 1912–1927.
40 X. Guan, F. Chen, Q. Fang and S. Qiu, *Chem. Soc. Rev.*, 2020, **49**, 1357–1384.
41 X. Guan, F. Chen, S. Qiu and Q. Fang, *Angew. Chem., Int. Ed.*, 2023, **62**, e202213203.
42 P. T. Phan, Q. T. H. Ta and P. K. T. Nguyen, *Polymers*, 2023, **15**, 887.
43 X. Han, C. Yuan, B. Hou, L. Liu, H. Li, Y. Liu and Y. Cui, *Chem. Soc. Rev.*, 2020, **49**, 6248–6272.
44 R. Freund, O. Zaremba, G. Arnauts, R. Ameloot, G. Skorupskii, M. Dinca, A. Bavykina, J. Gascon, A. Ejsmont, J. Goscianska, M. Kalmutzki, U. Lachelt, E. Ploetz, C. S. Diercks and S. Wuttke, *Angew. Chem., Int. Ed.*, 2021, **60**, 23975–24001.
45 H. Jiang, D. Alezi and M. Eddaoudi, *Nat. Rev. Mater.*, 2021, **6**, 466–487.
46 C. S. Diercks and O. M. Yaghi, *Science*, 2017, **355**, eaal1585.
47 H. Li, J. Ding, X. Guan, F. Chen, C. Li, L. Zhu, M. Xue, D. Yuan, V. Valtchev, Y. Yan, S. Qiu and Q. Fang, *J. Am. Chem. Soc.*, 2020, **142**, 13334–13338.
48 M. Martinez-Abadia, K. Strutynski, B. Lerma-Berlanga, C. T. Stoppiello, A. N. Khlobystov, C. Marti-Gastaldo, A. Saeki, M. Melle-Franco and A. Mateo-Alonso, *Angew. Chem., Int. Ed.*, 2021, **60**, 9941–9946.
49 W. Liu, L. Gong, Z. Liu, Y. Jin, H. Pan, X. Yang, B. Yu, N. Li, D. Qi, K. Wang, H. Wang and J. Jiang, *J. Am. Chem. Soc.*, 2022, **144**, 17209–17218.
50 Z. Shan, M. Wu, D. Zhu, X. Wu, K. Zhang, R. Verduzco and G. Zhang, *J. Am. Chem. Soc.*, 2022, **144**, 5728–5733.
51 K. Geng, T. He, R. Liu, S. Dalapati, K. T. Tan, Z. Li, S. Tao, Y. Gong, Q. Jiang and D. Jiang, *Chem. Rev.*, 2020, **120**, 8814–8933.
52 O. Delgado Friedrichs, M. O'Keeffe and O. M. Yaghi, *Acta Crystallogr., Sect. A: Found. Crystallogr.*, 2003, **59**, 22–27.
53 F. J. Uribe-Romo, J. R. Hunt, H. Furukawa, C. Klock, M. O'Keeffe and O. M. Yaghi, *J. Am. Chem. Soc.*, 2009, **131**, 4570–4571.
54 G. Lin, H. Ding, D. Yuan, B. Wang and C. Wang, *J. Am. Chem. Soc.*, 2016, **138**, 3302–3305.
55 Y. Zhang, J. Duan, D. Ma, P. Li, S. Li, H. Li, J. Zhou, X. Ma, X. Feng and B. Wang, *Angew. Chem., Int. Ed.*, 2017, **56**, 16313–16317.
56 O. Yahiaoui, A. N. Fitch, F. Hoffmann, M. Froba, A. Thomas and J. Roeser, *J. Am. Chem. Soc.*, 2018, **140**, 5330–5333.
57 H. L. Nguyen, C. Gropp, Y. Ma, C. Zhu and O. M. Yaghi, *J. Am. Chem. Soc.*, 2020, **142**, 20335–20339.
58 Z. Li, L. Sheng, H. Wang, X. Wang, M. Li, Y. Xu, H. Cui, H. Zhang, H. Liang, H. Xu and X. He, *J. Am. Chem. Soc.*, 2021, **143**, 92–96.
59 Z. Li, L. Sheng, C. Hsueh, X. Wang, H. Cui, H. Gao, Y. Wu, J. Wang, Y. Tang, H. Xu and X. He, *Chem. Mater.*, 2021, **33**, 9618–9623.
60 X. Wang, M. Bahri, Z. Fu, M. A. Little, L. Liu, H. Niu, N. D. Browning, S. Y. Chong, L. Chen, J. W. Ward and A. I. Cooper, *J. Am. Chem. Soc.*, 2021, **143**, 15011–15016.
61 H. S. Lu, W. K. Han, X. Yan, C. J. Chen, T. Niu and Z. G. Gu, *Angew. Chem., Int. Ed.*, 2021, **60**, 17881–17886.
62 F. Jin, E. Lin, T. Wang, S. Geng, L. Hao, Q. Zhu, Z. Wang, Y. Chen, P. Cheng and Z. Zhang, *J. Am. Chem. Soc.*, 2022, **144**, 23081–23088.
63 S. Das, T. Sekine, H. Mabuchi, T. Irie, J. Sakai, Y. Zhao, Q. Fang and Y. Negishi, *ACS Appl. Mater. Interfaces*, 2022, **14**, 48045–48051.
64 X. Xu, P. Cai, H. Chen, H. C. Zhou and N. Huang, *J. Am. Chem. Soc.*, 2022, **144**, 18511–18517.
65 W. K. Han, H. S. Lu, J. X. Fu, X. Liu, X. M. Zhu, X. D. Yan, J. W. Zhang, Y. Q. Jiang, H. L. Dong and Z. G. Gu, *Chem. Eng. J.*, 2022, **449**, 137802.
66 F. Jin, H. L. Nguyen, Z. Zhong, X. Han, C. Zhu, X. Pei, Y. Ma and O. M. Yaghi, *J. Am. Chem. Soc.*, 2022, **144**, 1539–1544.
67 R. Li, G. Xing, H. Li, S. Li and L. Chen, *Chin. Chem. Lett.*, 2023, **34**, 107454.
68 D. Zhu, Y. Zhu, Y. Chen, Q. Yan, H. Wu, C. Y. Liu, X. Wang, L. B. Alemany, G. Gao, T. P. Senftle, Y. Peng, X. Wu and R. Verduzco, *Nat. Commun.*, 2023, **14**, 2865.
69 M. M. Wu, Z. Shan, J. J. Wang, T. T. Liu and G. Zhang, *Chem. Eng. J.*, 2023, **454**, 140121.

70 S. J. Lyle, P. J. Waller and O. M. Yaghi, *Trends Chem.*, 2019, **1**, 172–184.
71 F. Haase and B. V. Lotsch, *Chem. Soc. Rev.*, 2020, **49**, 8469–8500.
72 B. Gui, J. Xin, Y. Cheng, Y. Zhang, G. Lin, P. Chen, J. X. Ma, X. Zhou, J. Sun and C. Wang, *J. Am. Chem. Soc.*, 2023, **145**, 11276–11281.
73 N. L. Campbell, R. Clowes, L. K. Ritchie and A. I. Cooper, *Chem. Mater.*, 2009, **21**, 204–206.
74 J. He, X. Jiang, F. Xu, C. Li, Z. Long, H. Chen and X. Hou, *Angew. Chem., Int. Ed.*, 2021, **60**, 9984–9989.
75 X. Guan, Y. Ma, H. Li, Y. Yusran, M. Xue, Q. Fang, Y. Yan, V. Valtchev and S. Qiu, *J. Am. Chem. Soc.*, 2018, **140**, 4494–4498.
76 J. Qiu, P. Guan, Y. Zhao, Z. Li, H. Wang and J. Wang, *Green Chem.*, 2020, **22**, 7537–7542.
77 D. Beaudoin, T. Maris and J. D. Wuest, *Nat. Chem.*, 2013, **5**, 830–834.
78 Y. B. Zhang, J. Su, H. Furukawa, Y. Yun, F. Gandara, A. Duong, X. Zou and O. M. Yaghi, *J. Am. Chem. Soc.*, 2013, **135**, 16336–16339.
79 A. M. Evans, I. Castano, A. Brumberg, L. R. Parent, A. R. Corcos, R. L. Li, N. C. Flanders, D. J. Gosztola, N. C. Gianneschi, R. D. Schaller and W. R. Dichtel, *J. Am. Chem. Soc.*, 2019, **141**, 19728–19735.
80 L. Peng, J. Sun, J. Huang, C. Song, Q. Wang, L. Wang, H. Yan, M. Ji, D. Wei, Y. Liu and D. Wei, *Chem. Mater.*, 2022, **34**, 2886–2895.
81 H. Furukawa and O. M. Yaghi, *J. Am. Chem. Soc.*, 2009, **131**, 8875–8883.
82 E. Klontzas, E. Tylianakis and G. E. Froudakis, *Nano Lett.*, 2010, **10**, 452–454.
83 C. Yu, H. Li, Y. Wang, J. Suo, X. Guan, R. Wang, V. Valtchev, Y. Yan, S. Qiu and Q. Fang, *Angew. Chem., Int. Ed.*, 2022, **61**, e202117101.
84 J. Lan, D. Cao and W. Wang, *Langmuir*, 2010, **26**, 220–226.
85 J. L. Mendoza-Cortes, T. A. Pascal and W. A. Goddard III, *J. Phys. Chem. A*, 2011, **115**, 13852–13857.
86 R. Mercado, R.-S. Fu, A. V. Yakutovich, L. Talirz, M. Haranczyk and B. Smit, *Chem. Mater.*, 2018, **30**, 5069–5086.
87 P. Guan, J. Qiu, Y. Zhao, H. Wang, Z. Li, Y. Shi and J. Wang, *Chem. Commun.*, 2019, **55**, 12459–12462.
88 C. Wang, Y. Wang, R. Ge, X. Song, X. Xing, Q. Jiang, H. Lu, C. Hao, X. Guo, Y. Gao and D. Jiang, *Chem. – Eur. J.*, 2018, **24**, 585–589.
89 J. Zou, D. Wen and Y. Zhao, *Dalton Trans.*, 2023, **52**, 731–736.
90 J. Chang, H. Li, J. Zhao, X. Guan, C. Li, G. Yu, V. Valtchev, Y. Yan, S. Qiu and Q. Fang, *Chem. Sci.*, 2021, **12**, 8452–8457.
91 F. Jin, E. Lin, T. Wang, S. Geng, T. Wang, W. Liu, F. Xiong, Z. Wang, Y. Chen, P. Cheng and Z. Zhang, *J. Am. Chem. Soc.*, 2022, **144**, 5643–5652.
92 Y. Cheng, L. Zhai, Y. Ying, Y. Wang, G. Liu, J. Dong, D. Z. L. Ng, S. A. Khan and D. Zhao, *J. Mater. Chem. A*, 2019, **7**, 4549–4560.
93 H. Lu, C. Wang, J. Chen, R. Ge, W. Leng, B. Dong, J. Huang and Y. Gao, *Chem. Commun.*, 2015, **51**, 15562–15565.
94 S. Yan, X. Guan, H. Li, D. Li, M. Xue, Y. Yan, V. Valtchev, S. Qiu and Q. Fang, *J. Am. Chem. Soc.*, 2019, **141**, 2920–2924.
95 G. Lin, H. Ding, R. Chen, Z. Peng, B. Wang and C. Wang, *J. Am. Chem. Soc.*, 2017, **139**, 8705–8709.
96 S.-Y. Chi, Q. Chen, S.-S. Zhao, D.-H. Si, Q.-J. Wu, Y.-B. Huang and R. Cao, *J. Mater. Chem. A*, 2022, **10**, 4653–4659.
97 B. Han, Y. Jin, B. Chen, W. Zhou, B. Yu, C. Wei, H. Wang, K. Wang, Y. Chen, B. Chen and J. Jiang, *Angew. Chem., Int. Ed.*, 2022, **61**, e202114244.
98 Q. Fang, S. Gu, J. Zheng, Z. Zhuang, S. Qiu and Y. Yan, *Angew. Chem., Int. Ed.*, 2014, **53**, 2878–2882.
99 H. Li, Q. Pan, Y. Ma, X. Guan, M. Xue, Q. Fang, Y. Yan, V. Valtchev and S. Qiu, *J. Am. Chem. Soc.*, 2016, **138**, 14783–14788.
100 J. Luis-Barrerra, R. Cano, G. Imani-Shakibaei, J. Heras-Domingo, J. Pérez-Carvajal, I. Imaz, D. Maspoch, X. Solans-Monfort, J. Alemán and R. Mas-Ballesté, *Catal. Sci. Technol.*, 2019, **9**, 6007–6014.
101 H. Ding, J. Li, G. Xie, G. Lin, R. Chen, Z. Peng, C. Yang, B. Wang, J. Sun and C. Wang, *Nat. Commun.*, 2018, **9**, 5234.
102 J. Fang, Z. Fu, X. Chen, Y. Liu, F. Chen, Y. Wang, H. Li, Y. Yusran, K. Wang, V. Valtchev, S. Qiu, B. Zou and Q. Fang, *Angew. Chem., Int. Ed.*, 2023, **62**, e202304234.
103 W.-R. Cui, Y.-R. Chen, W. Xu, K. Liu, W.-B. Qiu, Y. Li and J.-D. Qiu, *Sep. Purif. Technol.*, 2023, **306**, 122726.
104 M. Li, Z. Cui, S. Pang, L. Meng, D. Ma, Y. Li, Z. Shi and S. Feng, *J. Mater. Chem. C*, 2019, **7**, 11919–11925.
105 Y. Y. Liu, X. C. Li, S. Wang, T. Cheng, H. Yang, C. Liu, Y. Gong, W. Y. Lai and W. Huang, *Nat. Commun.*, 2020, **11**, 5561.
106 Z. Mei, H. Li, G. Wang, Y. Mao, Y. Xu, J. Guo, Q. Li, H. Li, W. Li, Y. Tang and X. Liang, *Appl. Surf. Sci.*, 2023, **615**, 156324.
107 T. Jadhav, Y. Fang, C.-H. Liu, A. Dadvand, E. Hamzehpoor, W. Patterson, A. Jonderian, R. S. Stein and D. F. Perepichka, *J. Am. Chem. Soc.*, 2020, **142**, 8862–8870.
108 H. Li, J. Chang, S. Li, X. Guan, D. Li, C. Li, L. Tang, M. Xue, Y. Yan, V. Valtchev, S. Qiu and Q. Fang, *J. Am. Chem. Soc.*, 2019, **141**, 13324–13329.
109 Y. Liu, Y. Feng, Z. Huang and X. Zhang, *J. Phys. Chem. C*, 2016, **120**, 17060–17068.
110 S. K. S. Freitas, R. S. Borges, C. Merlini, G. M. O. Barra and P. M. Esteves, *J. Phys. Chem. C*, 2017, **121**, 27247–27252.
111 H. Ma, Z. Aamer and Z. Tian, *Mater. Today Phys.*, 2021, **21**, 100536.
112 Q. Fang, J. Wang, S. Gu, R. B. Kaspar, Z. Zhuang, J. Zheng, H. Guo, S. Qiu and Y. Yan, *J. Am. Chem. Soc.*, 2015, **137**, 8352–8355.
113 Y. Zhao, S. Das, T. Sekine, H. Mabuchi, T. Irie, J. Sakai, D. Wen, W. Zhu, T. Ben and Y. Negishi, *Angew. Chem., Int. Ed.*, 2023, **62**, e202300172.
114 W. Zhao, C. Yu, J. Zhao, F. Chen, X. Guan, H. Li, B. Tang, G. Yu, V. Valtchev, Y. Yan, S. Qiu and Q. Fang, *Small*, 2021, **17**, 2102630.

